Partial cross sections for excitation of He($3\,^1D$) states by electron impact

A. G. Mikosza, R. Hippler,* J. B. Wang, and J. F. Williams
Physics Department, The University of Western Australia, Nedlands, Perth 6907, Australia
(Received 14 April 1995; revised manuscript received 12 September 1995)

We report absolute measurements of a rank four state multipole for He($3\,^1D$) excitation by electron impact with a polarized first-photon–second-photon coincidence technique. The presented technique permits the extraction of total (scattering angle integrated) partial cross sections σ_m for the excitation of He($3\,^1D_m$) magnetic substates ($m=0,\pm1,\pm2$). The present results stringently test existing theories and, for example, indicate that most theoretical calculations underestimate the partial cross sections σ_0 and σ_1 and overestimate the σ_2. The recent convergent close-coupling calculations of Fursa and Bray [Phys. Rev. A **52**, 1279 (1995)] are in excellent agreement with all our measured data.

PACS number(s): 34.80.Dp

I. INTRODUCTION

Experimental and theoretical investigations of electron collisions with atoms are of considerable importance for our understanding of quantum scattering processes both from a fundamental and applied point of view. For the latter case, the deduced information has applications in astrophysics, stellar and planetary atmospheres, laser physics, and plasma physics. Knowledge at the fundamental level is also required for a better understanding of the underlying microscopic processes and of the interactions involved in such collisions. The excitation of helium by electron impact provides particularly valuable information as a prototype case for the study of coherent excitation processes. Previous investigations in the field have concentrated on the excitation of He ($n\,^1P$) states and only recently more work has been devoted to the excitation of other states [1]. Many of these later investigations relied on the scattered electron-emitted photon coincidence technique, which allows for a detailed analysis of the collision event in terms of scattering amplitudes and their respective phases. For the excitation of He($n\,^1P$) states the scattering amplitudes can be fully determined and any incoherence, caused by whatever reason, can at least, in principle, be detected. However, for the He($3\,^1D$) state, the angular and polarization correlation measurements of only the scattered electron and either the first or second cascade photon are insufficient to determine, in the natural frame, the three amplitudes, their two relative phases and the phase ambiguity between the $m=\pm2$ amplitudes. This paper now discusses the measurements between pairs of outgoing particles and outlines the theoretical framework required for the triple coincidence measurements.

In the ordinary scattered electron-emitted photon coincidence technique the linear and circular polarizations of only one photon from the $3\,^1D\rightarrow2\,^1P$ transition are exploited. Our newly developed photon-photon coincidence technique also provides the information on the intermediate He($2\,^1P$) state through the detection of the $2\,^1P\rightarrow1\,^1S$ transition by which the excited He($3\,^1D$) state ultimately decays to the ground state. This two-photon coincidence when combined with the detection of a scattered electron to give a triple coincidence technique provides the additional information required to completely characterize the excited He($3\,^1D$) charge cloud and thereby allows extraction of the maximum information possible from such kind of scattering experiment. Since the experimental realization has only recently progressed to the state where the triple coincidence experiment actually becomes feasible [2], we present results here for the two-photon coincidence from which the state multipoles $\langle T(2)_{K0}\rangle$ ($K=0,2,4$) are derived. The state multipoles describe the population and the anisotropy of the excited He($3\,^1D_m$) state and are related to the partial cross sections σ_m for the excitation of the He($3\,^1D_m$) magnetic substates ($m=0,\pm1,\pm2$). The technique described here was introduced by Williams, Kumar, and Stelbovics [3] for electron-impact studies yielding excited H($n=3$) hydrogen atoms. The selection of helium compared to atomic hydrogen offers several advantages. In helium, the first photon from the $3\,^1D\rightarrow2\,^1P$ transition is uniquely selected by a wavelength filter that is not feasible with hydrogen because of the H($n=3$) degeneracy. The results presented here were obtained by exploiting the polarization properties of the first (γ_1) photon in coincidence with the second photon (γ_2) whose detector remained fixed during the measurements. This method provides a much higher degree of statistical significance compared to the two-photon angular-correlation work of Williams, Kumar, and Stelbovics [3]. Further, since the total electronic and nuclear spins are zero in helium, the present investigation does not suffer from depolarization effects due to fine and hyperfine interactions during the decay of the excited atoms. A preliminary account of the present work has been given in a recent letter [4].

II. THEORY

The experimental polarization correlations can be related to the state multipoles $\langle T(2)_{KQ}\rangle$ with rank K up to 4. The theoretical analysis of the sequential two-photon cascade emitted during the decay of excited atoms needs three equations. The first equation describes the time evolution of the excited atom under its total Hamiltonian. The second equation describes the configuration of the intermediate state of

*Permanent address: Institut für Physik, Universität Greifswald, Domstrasse 10a, D-17487 Greifswald, Germany.

the atom to which it has decayed immediately after the emission of the first photon, and the third equation provides the density matrix of the emitted photons. Wang *et al.* [5] presented a general theoretical description of such sequential cascades that rests on the works of Fano and Macek [6], Blum and Kleinpoppen [7,8], and Heck and Gauntlett [9]. The present work involves measurements of the cascading photons from $3\,^1D \rightarrow 2\,^1P \rightarrow 1\,^1S$ singlet states of helium where both the total electronic and nuclear spins are zero. In this case, the time evolution of the state multipoles $\langle T(L_2;t)^\dagger_{kq}\rangle$ (with $L_2=2$ for a $3\,^1D$ state) simplifies to

$$\langle T(L_2;t)^\dagger_{kq}\rangle = \langle T(L_2;t=0)^\dagger_{kq}\rangle e^{-\gamma_1 t}. \tag{1}$$

After some finite time $t=t_1$ the excited atom decays from its upper $3\,^1D$ ($L_2=2$) state to the intermediate $2\,^1P$ ($L_1=1$) state, where γ_1 is the decay constant of the upper state. In the dipole approximation, the intermediate state is described by

$$\begin{aligned}\langle T(L_1;t_1\lambda_1\lambda_1'\vec{n}_1)^\dagger_{KQ}\rangle_{\rm lab} &= C(\omega_1)\sum_{kqpa}\langle T(L_2;t_1)^\dagger_{kq}\rangle_{\rm lab}\mathbf{D}(0\,\theta_1\phi_1)^{(k)}_{pq}{\rm Tr}\{r_{-\lambda_1}T(L_2)_{kp}r^\dagger_{-\lambda_1'}T(L_1)^\dagger_{Ka}\}_{\vec{n}_1}\mathbf{D}^*(0\,\theta_1\phi_1)^{(K)}_{aQ}\\ &= C(\omega_1)e^{-\gamma_1 t_1}|\langle L_1\|\vec{r}\|L_2\rangle|^2\sqrt{2K+1}\sum_{kqabp}(-1)^{k+a}(2b+1)\sqrt{2k+1}\begin{pmatrix} k & b & K\\ -p & \lambda_1-\lambda_1' & a\end{pmatrix}\\ &\times\begin{pmatrix} b & 1 & 1\\ \lambda_1-\lambda_1' & \lambda_1' & -\lambda_1\end{pmatrix}\begin{Bmatrix} k & b & K\\ L_2 & 1 & L_1\\ L_2 & 1 & L_1\end{Bmatrix}\langle T(L_2)^\dagger_{kq}\rangle_{\rm lab}\mathbf{D}(0\,\theta_1\phi_1)^{(k)}_{pq}\mathbf{D}^*(0\,\theta_1\phi_1)^{(K)}_{aQ},\end{aligned} \tag{2}$$

where λ_1, ω_1, and (θ_1,ϕ_1) are, respectively, the helicity, frequency, and Euler angles of the first emitted photon. $\mathbf{D}$ is the rotation matrix as defined by Edmonds [10]. The intermediate ($L_1=1$) state will decay to the lower $1\,^1S$ ($L_0=0$) state at a later time t_2, emitting a second photon along the direction $\vec{n}_2(\theta_2,\phi_2)$ and with helicity λ_2, and frequency ω_2. All polar angles (θ_1,θ_2) are measured here relative to the direction of the incident electron, while the azimuthal angles (ϕ_1,ϕ_2) are defined with respect to the scattering plane given by the incident and the outgoing directions of the scattered electron (*collision frame*). Equation (2) applies to the elementary process in which the scattered electron is detected in coincidence with both cascading photons from the $3\,^1D \rightarrow 2\,^1P \rightarrow 1\,^1S$ decay (so-called triple coincidence experiment). The density matrix describing the polarization states of the two photons is given by

$$\begin{aligned}\rho(t_1\lambda_1\lambda_1'\vec{n}_1,t_2\lambda_2\lambda_2'\vec{n}_2) &= C(\omega_2)\sum_{KQQ'}\langle T(L_1;t_2,t_1,\lambda_1\lambda_1'\vec{n}_1)^\dagger_{KQ}\rangle_{\rm lab}\mathbf{D}(0\,\theta_2\phi_2)^{(K)}_{Q'Q}{\rm Tr}\{r_{-\lambda_2}T(L_1)_{KQ'}r^\dagger_{-\lambda_2'}\}_{\vec{n}_2}\\ &= C(\omega_2)(-1)^{\lambda_2}e^{-\gamma_2 t_2}|\langle L_0\|\vec{r}\|L_1\rangle|^2\sum_{KQQ'}\sqrt{2K+1}\begin{pmatrix} 1 & 1 & K\\ -\lambda_2' & \lambda_2 & Q'\end{pmatrix}\begin{Bmatrix} 1 & 1 & K\\ L_1 & L_1 & L_0\end{Bmatrix}\\ &\times\langle T(L_1;t_1\lambda_1\lambda_1'\vec{n}_1)^\dagger_{KQ}\rangle_{\rm lab}\mathbf{D}(0\,\theta_2\phi_2)^{(K)}_{Q'Q}.\end{aligned} \tag{3}$$

The coincidence intensity is obtained by summing the above equation over the helicities of both photons:

$$I(\theta_1\phi_1\theta_2\phi_2,t_1t_2) = \sum_{\substack{\lambda_1=\lambda_1'=\pm1\\ \lambda_2=\lambda_2'=\pm1}}\rho(t_1\lambda_1\lambda_1'\vec{n}_1,t_2\lambda_2\lambda_2'\vec{n}_2) = C'(\omega_1\omega_2t_1t_2)\sum_{kq}I_{kq}(\theta_1\phi_1\theta_2\phi_2)\langle T(L_2)^\dagger_{kq}\rangle_{\rm lab}, \tag{4}$$

where the I_{kq} include all the Clebsch-Gordan sums and the angle-dependent terms. The various polarization parameters are obtained by different combinations of the density-matrix elements. In the present work, where the first polarized photon and the unpolarized second photon were measured in coincidence, the Stokes parameters are given by

$$IP_1 = -\sum_{\lambda_1=\lambda_1'=\pm1}[\rho(\lambda_2=-1;\lambda_2'=1) + \rho(\lambda_2=1;\lambda_2'=-1)], \tag{5a}$$

$$IP_2 = i\sum_{\lambda_1=\lambda_1'=\pm1}[\rho(\lambda_2=-1;\lambda_2'=1) - \rho(\lambda_2=1;\lambda_2'=-1)], \tag{5b}$$

$$IP_3 = \sum_{\lambda_1=\lambda_1'=\pm1}[\rho(\lambda_2=1;\lambda_2'=1) - \rho(\lambda_2=-1;\lambda_2'=-1)]. \tag{5c}$$

In order to obtain the two-photon coincidence signal, i.e., for the integral process in which the scattered electron is not

detected, we integrate Eqs. (4) and (5) over the direction of the (unobserved) scattered electron. The explicit expressions for the linear and circular polarization IP_i $(i=1-3)$ of the first photon detected in coincidence with the second photon, obtained for the geometry employed in the present work $(\theta_1=\theta_2=90°)$, are given as

$$IP_1=\frac{3\sin^2(\phi_1-\phi_2)}{4\sqrt{5}}\langle T(2)_{00}\rangle - \frac{39-3\cos2(\phi_1-\phi_2)}{4\sqrt{14}}\langle T(2)_{20}\rangle + \frac{54-9\cos2(\phi_1-\phi_2)}{4\sqrt{70}}\langle T(2)_{40}\rangle, \tag{6a}$$

$$IP_2=0, \tag{6b}$$

$$IP_3=0, \tag{6c}$$

where

$$I=\frac{81+3\cos2(\phi_1-\phi_2)}{8\sqrt{5}}\langle T(2)_{00}\rangle + \frac{27+3\cos2(\phi_1-\phi_2)}{4\sqrt{14}}\langle T(2)_{20}\rangle + \frac{18+9\cos2(\phi_1-\phi_2)}{4\sqrt{70}}\langle T(2)_{40}\rangle. \tag{6d}$$

Using Eqs. (6) and performing measurements at a minimum of two combinations of the relative azimuthal angles $\Delta\phi=\phi_1-\phi_2$, we can extract all the state multipoles up to rank $K=4$. Since there is rotational symmetry about the incident electron axis, all states multipoles $\langle T(2)_{KQ}\rangle$ with K odd and $Q\neq0$ are zero. Of the remaining three state multipoles $\langle T(2)_{K0}\rangle$ $K=0,2,4$, the two state multipoles $\langle T(2)_{00}\rangle$ and $\langle T(2)_{20}\rangle$ with rank $K=0$ and 2, respectively, are more easily and more precisely obtained from the noncoincident intensity and linear polarization of the first photon than from a two-photon coincidence experiment. Then

$$I^{(\gamma_1)}P^{(\gamma_1)}=\frac{3\sqrt{14}}{8}\langle T(2)_{20}\rangle, \tag{7a}$$

$$I^{(\gamma_1)}=\sqrt{5}\langle T(2)_{00}\rangle-\frac{\sqrt{14}}{8}\langle T(2)_{20}\rangle. \tag{7b}$$

Here the linear (P_1,P_2) and circular polarizations (P_3) or Stokes parameters are defined in the usual way [1],

$$P_1=\frac{I(0°)-I(90°)}{I(0°)+I(90°)}, \tag{8a}$$

$$P_2=\frac{I(45°)-I(135°)}{I(45°)+I(135°)}, \tag{8b}$$

$$P_3=\frac{I(-)-I(+)}{I(-)+I(+)}, \tag{8c}$$

where $I(\alpha)$ relates to the intensity with the linear polarizer's axis forming an angle α with respect to the z axis chosen as the direction of the incident electron. Also, $I(+)$ and $I(-)$ are the intensities of circularly polarized light with positive and negative helicity, respectively.

Then combining Eqs. (6) and (7) we may completely determine all three state multipoles describing the excited He($3\,^1D$) state. As mentioned before, the state multipoles relate to the partial cross sections σ_m for excitation of a particular $|D_m\rangle$ substate $(m=0,\pm1,\pm2)$.

$$\langle T(2)_{00}\rangle=\sqrt{\tfrac{1}{5}}(\sigma_0+2\sigma_1+\sigma_2), \tag{9a}$$

$$\langle T(2)_{20}\rangle=-\sqrt{\tfrac{2}{7}}(\sigma_0+\sigma_1-2\sigma_2), \tag{9b}$$

$$\langle T(2)_{40}\rangle=\sqrt{\tfrac{2}{35}}(3\sigma_0-4\sigma_1+\sigma_2). \tag{9c}$$

For symmetry reasons, $\sigma_m=\sigma_{-m}$ [8].

III. EXPERIMENTAL SET-UP

The experimental method, as indicated in Fig. 1, involves electron-impact excitation of helium target atoms and the coincident detection of two photons following the decay of the excited He($3\,^1D$) state via the intermediate He($2\,^1P$) to the He($1\,^1S$) ground state. The apparatus used in this work has been build and extensively modified over more than 15 years [11,12]. It consists of a cylindrical vacuum chamber with built-in rotary tables and mounts for the electron gun, a moveable Faraday cup, the electrostatic electron energy analyzer (not used in the present experiment), and the in-the-scattering-plane vacuum ultraviolet (vuv) photon detector. In addition, two photon detectors for visible photons have been added. These are located outside the collision chamber and view the collision region perpendicular to the electron-beam direction and either perpendicular (vertical) or parallel (horizontal), respectively, to the collision plane. The latest mechanical modifications to the apparatus have resulted in pre-

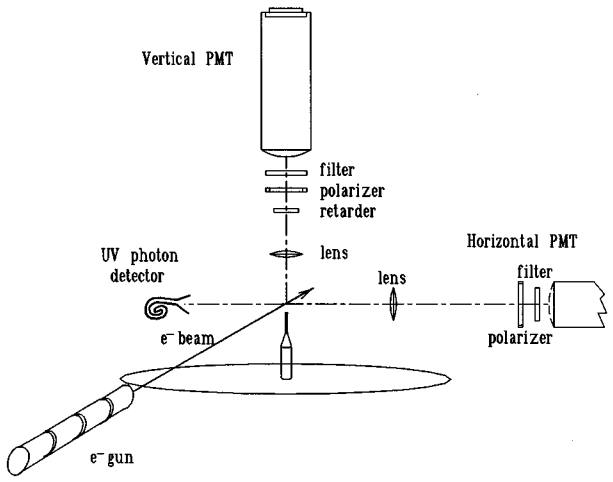

FIG. 1. Schematic representation of the experimental setup.

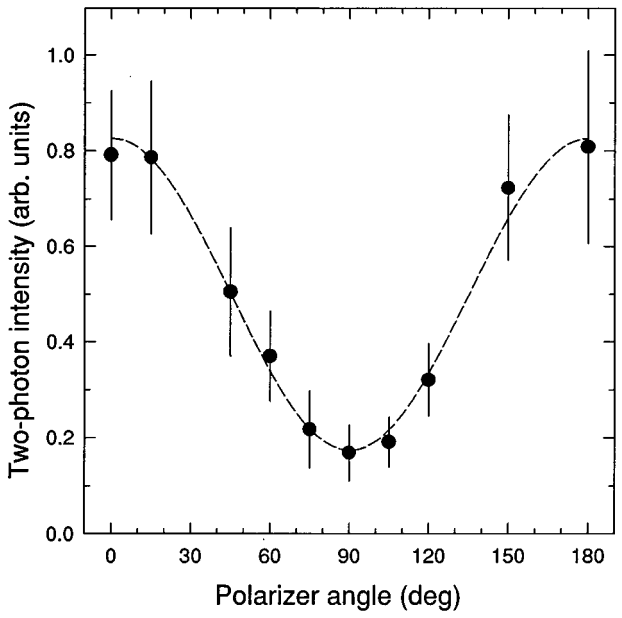

FIG. 2. Two-photon polarization correlation of the first (visible) photon detected in coincidence with the second (vuv) photon vs polarizer angle α at an incident energy $E=50$ eV. The experimental results (●) and a least-squares fit of Eq. (10) to the experimental data points are shown. The errors represent one standard deviation.

cision geometric locations of all components to within 0.1 mm.

The vacuum chamber is pumped to a base pressure of 6×10^{-8} Torr by a 1000 1/s diffusion pump equipped with a liquid nitrogen-cooled baffle and backed by a rotary pump. Electrons are produced inside the chamber by an electron gun consisting of an indirectly heated BaO cathode followed by a three-element condenser lens and a five-element variable zoom lens. The electron-beam energy width is about 0.4 eV and typical beam currents in the present experiment ranged between 0.2–0.5 μA. Recent modifications to the electron gun include an extra set of vertical and horizontal deflection plates located in the zoom section of the electron gun that allow for an improved positioning of the electron beam within 0.1 mm relative to the rotary axis of the tables. The helium target gas effused from a single capillary with a 0.3 mm diam. and 5 mm length located in the center of the rotary tables. Typical driving pressures behind the capillary were 0.2–0.5 Torr, resulting in a background pressure of about 1×10^{-7} Torr. This pressure was found to be low enough for pressure-dependent effects due to resonance trapping arising from the absorption and subsequent re-emission of the emitted $2\,^1P\rightarrow1\,^1S$ (58.4 nm) photons to be negligible for the present type of measurements [12].

The main modification for the present experiment involves the simultaneous detection of two photons. The first (visible) photon (γ_1) originates from the $\mathrm{He}(3\,^1D)\rightarrow\mathrm{He}(2\,^1P)$ transition at 667.8 nm. These photons were selected by an optical lens (entrance solid angle 0.144 sr) to form a parallel beam of light that was subsequently directed onto the appropriate retarder and linear polarizer combination to permit a full polarization analysis of the emitted light. The polarizer was followed by an interference filter and a photomultiplier tube (Thorn-Emi 9863QB) cooled to about -15°C and operated in the pulse-counting mode. Two different visible polarizer/detector systems have been used. These were located outside the collision chamber but placed either vertical or horizontal with respect to the rotary table with the electron gun. The polarimetry components and tests carried out to ensure the proper handedness of the retarders were described in detail by Wedding, Mikosza, and Williams [13]. The second (vacuum ultraviolet, vuv) photon (γ_2) from the subsequent $\mathrm{He}(2\,^1P)\rightarrow\mathrm{He}(1\,^1S)$ decay at 58.4 nm passed through an entrance solid angle of 0.03 sr in front of a Mullard B418BL channel electron multiplier. During the course of measurements this entrance solid angle was increased to 0.12 sr. No polarization analysis was carried out for this second photon. All (visible and vuv) photons were detected perpendicular to the electron beam ($\theta_1=\theta_2=90°$). The relative (azimuthal) angle $\Delta\phi=\phi_1-\phi_2$ between the visible (γ_1) and the vuv (γ_2) photon was chosen as $\Delta\phi=90°$ and $\Delta\phi=180°$ for the vertical and horizontal visible photon detection systems, respectively.

The output signals from the photon detectors were suitably amplified by fast amplifiers and the required timing information was obtained from fast discriminators that provided the start and stop signals for the time-to-amplitude converter (TAC). Standard coincidence electronics have been used throughout, with a coincidence-resolving time of about 1.5 nsec. The time coincidence spectra were recorded with a Canberra S100 pulse-height analyzer controlled by an AT-486 personal computer, permitting on-line data storage and analysis.

In any practical coincidence measurement, the angular resolutions of the detectors are finite. The acceptance angles chosen above were small enough to avoid any corrections due to the finite solid angles and yet were large enough to provide reasonable counting statistics in reasonable counting times, typically 2–3 days per data point.

IV. RESULTS AND DISCUSSION

A typical result for the coincident two-photon intensity $I(\alpha)$ with the two-photon detectors perpendicular to the electron beam ($\theta_1=\theta_2=90°$) and perpendicular to each other ($\Delta\phi=90°$), measured as a function of polarizer angle α is shown in Fig. 2. The incident-electron energy was $E=50$ eV. All quoted angles refer to the z axis chosen as the direction of the incident electron. The data display a pronounced polarization correlation of the first photon (γ_1) measured in coincidence with the second photon (γ_2), which is symmetric about the incident electron axis. From a least-squares fit to these data using

$$I(\alpha)=\tfrac{1}{2}I_0(1+P_1\cos2\alpha+P_2\sin2\alpha), \tag{10}$$

where I_0 is the total two-photon intensity, we obtain $P_1=0.652\pm0.029$ and $P_2=0.005\pm0.032$. A previous measurement at 81.6 eV yielded $P_1=0.458\pm0.057$ and $P_2=-0.005\pm0.058$ [4]. For the circular polarization P_3 that was measured separately at 81.6 eV we obtained $P_3=-0.022\pm0.097$ [4]. For the experimental conditions chosen here, symmetry predicts $P_2=P_3=0$ (see above), which is in agreement with experiment.

TABLE I. Coincident two-photon [P_1, Eq. (6)] and the noncoincident one-photon [$P_1^{(\gamma_1)}$, Eq. (7)] polarization correlation, and the extracted normalized rank $K=2$ and 4 state multipoles $\langle t_{K0}\rangle=\langle T(2)_{K0}\rangle/\langle T(2)_{00}\rangle$ for the investigated incident energies $E=40$–300 eV. The relative azimuthal angle $\Delta\phi$ between the two photon detectors was 90° except for the indicated $E=40$ eV measurement (†), where it was 180°.

E (eV)	P_1	$P_1^{(\gamma_1)}$	$\langle t_{20}\rangle$	$\langle t_{40}\rangle$
40	0.753±0.058	0.484±0.01	−0.920±0.023	0.878±0.211
40†	0.447±0.036	0.484±0.01	−0.920±0.023	0.725±0.256
50	0.664±0.026	0.470±0.01	−0.887±0.022	0.595±0.092
60	0.627±0.108	0.437±0.015	−0.815±0.033	0.543±0.370
81.6	0.458±0.058	0.347±0.015	−0.626±0.031	0.207±0.182
100	0.358±0.071	0.303±0.015	−0.537±0.030	0.015±0.211
150	0.254±0.072	0.157±0.01	−0.265±0.018	0.077±0.191
200	0.248±0.088	0.093±0.01	−0.153±0.017	0.209±0.227
250		0.049±0.01	−0.079±0.016	
300		0.013±0.01	−0.020±0.016	

To extract the relative tensor $\langle t_{K0}\rangle=\langle T(2)_{K0}\rangle/\langle T(2)_{00}\rangle$ ($K=2,4$) from the measured polarization correlations, at least two independent polarization measurements are required. In order to determine the relative tensor of rank $K=2$, $\langle t_{20}\rangle=\langle T(2)_{20}\rangle/\langle T(2)_{00}\rangle$ suffices to measure the one-photon polarization $P_1^{(\gamma_1)}$ of the first γ_1 photon. This does not require a coincidence measurement and, hence, has the advantage that the required linear polarization $P_1^{(\gamma_1)}$ can be measured with high precision easing the data handling considerably. The measured one-photon polarizations are given in Table I and are found to agree excellently over the entire energy range from 40 to 300 eV with previous experimental results by McLaughlin and Crowe [14]. On the other hand, tensors of rank $K>2$ cannot be obtained from one-photon experiments. The determination of a rank $K=4$ tensor therefore requires at least one two-photon polarization or angular correlation measurement in addition to the one-photon polarization $P_1^{(\gamma_1)}$. Combining these two (one- and two-photon) measurements using Eqs. (6) and (7), we obtain the relative tensors $\langle t_{K0}\rangle=\langle T(2)_{K0}\rangle/\langle T(2)_{00}\rangle$ ($K=2,4$), which are given in Table I.

A major problem in placing the above state multipoles on an absolute scale, which is the determination of absolute cross sections, is the calibration of the photon detection system. Previous attempts to measure absolute cross sections include the works of Gabriel and Heddle [15], St. John, Miller, and Lin [16], Moussa, de Heer, and Schutten [17], and Showalter and Kay [18]. These experiments yielded cross sections that are considerably larger than the previously available calculations based on various models, e.g., first Born approximation (FBA) [19,20] 22-state second-order diagonalization method (SOD) [21], ten-state eikonal calculation [22], multichannel eikonal theory (DMET) [23], and distorted-wave Born approximation with excited-state distorting potentials (DWBA-EP) [24]. de Heer *et al.* [25,26] have made a critical evaluation of the then available data sets and recommended a data base which, for the He($3\,^1D$) excitation, is relatively close to experiment around 100 eV but approaches theory around 1 keV. While we did not attempt to carry out an absolute intensity calibration, we have carried out a relative measurement of the total He($3\,^1D$) cross section as a function of energy and, at a selected energy of 100 eV, with respect to the cross section for He($3\,^1S$) excitation. The latter comparison is facilitated by the fact that experiment and theory agree well for excitation of the He($3\,^1S$) state, and that the corresponding radiative transitions at 667.8 and 728.1 nm are relatively close to each other. Using absolute quantum efficiencies (4.15% at 667.8 nm and 1.35% at 728.1 nm) provided by the manufacturer of the multiplier (Thorn-Emi 9863 QB) used in the present experiment, and

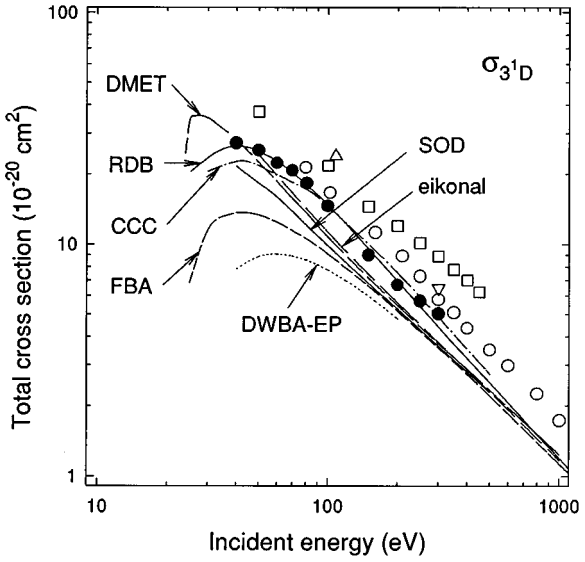

FIG. 3. Total cross section $\sigma_{3\,^1D}$ vs incident energy. Experiment: present relative measurements (●) normalized to the recommended data set of de Heer *et al.* [25]; absolute measurements of Gabriel and Heddle (△, Ref. [15]), St. John, Miller, and Lin (□, Ref. [16]), Moussa, de Heer, and Schutten (○, Ref. [17]), and Showalter and Kay (▽, Ref. [18]). Theory: first Born approximation (FBA) calculations [19,20], distorted-wave Born approximation with excited-state distorting potentials (DWBA-EP, Ref. [24]), 22-state second-order diagonalization method (SOD, Ref. [21]), ten-state eikonal calculations (eikonal, Ref. [22]), multichannel eikonal theory (DMET, Ref. [23]), and the convergent close-coupling method (CCC, Ref. [27]). The solid curve is from the recommended data base of de Heer *et al.* (RDB, Ref. [25]).

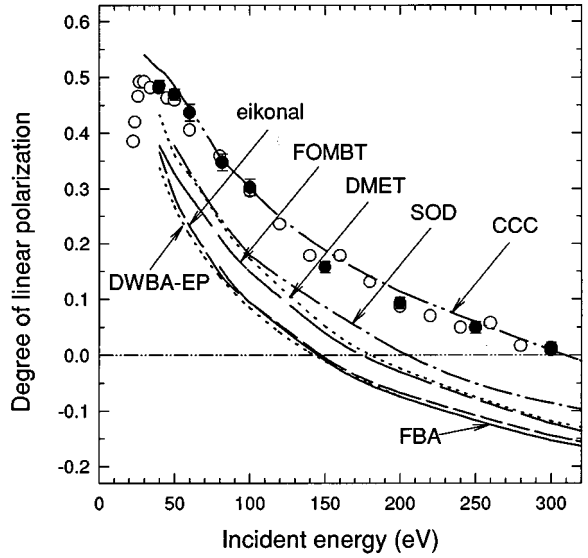

FIG. 4. Measured integral polarization P_1 for He($3\,^1D$) excitation by electron impact. The present experimental results (●) are compared with measurements of Crowe and McLaughlin (○) and with theoretical calculations employing the first Born approximation (FBA, Refs. [19,20]), ten-state eikonal calculations (eikonal, Ref. [22]), first-order many-body theory (FOMBT, Ref. [29]), multichannel eikonal theory (DMET, Ref. [23]), 22-state second-order diagonalization method (SOD, Ref. [21]), and the convergent close-coupling method (CCC, Ref. [27]).

measured transmission curves (52% at 667.8 nm and 80% at 728.1 nm) for the interference filters of interest here, we measured, at 100 eV incident energy, a cross-section ratio $\sigma(3\,^1D)/\sigma(3\,^1S)=0.66$. This measured ratio is close to the recommended ratio $\sigma(3\,^1D)/\sigma(3\,^1S)=0.64$ from the cross-section data base of de Heer *et al.* [25]. In this and in the following comparison, the anisotropic emission of the emitted photons using the measured integral polarization (Table I), and the cascade corrections proposed by Moussa, de Heer, and Schutten [17] were taken into account. In the light of this fair agreement, we have normalized our relative cross sections at 100 eV to the recommended data base (RDB) of de Heer *et al.* [25]. As can be concluded from Fig. 3, these normalized cross sections agree reasonably with this data base over the investigated energy of 40 up to 300 eV. The previous theoretical calculations are found to deviate in varying degree from the present data and sometimes by factors larger than 2. Since then, a very recent calculation by Fursa and Bray [27] has been published. The calculation employs the convergent close-coupling (CCC) method of Bray and Stelbovics [28] and in addition to bound states also takes continuum states into account. The new calculation shows excellent agreement with the present results and with the recommended data base of de Heer *et al.* [25].

Significant deviations to most theoretical calculations are also observed for the measured one-photon polarizations $P_1^{(\gamma_1)}$, which are displayed in Fig. 4. While there is excellent agreement of the present results with previous measurements of McLaughlin and Crowe [14], considerable discrepancies are noted with calculations based on the above theoretical models [19,21–23], including the first-order many-body theory (FOMBT) results of Csanak and Cartwright [29]. In

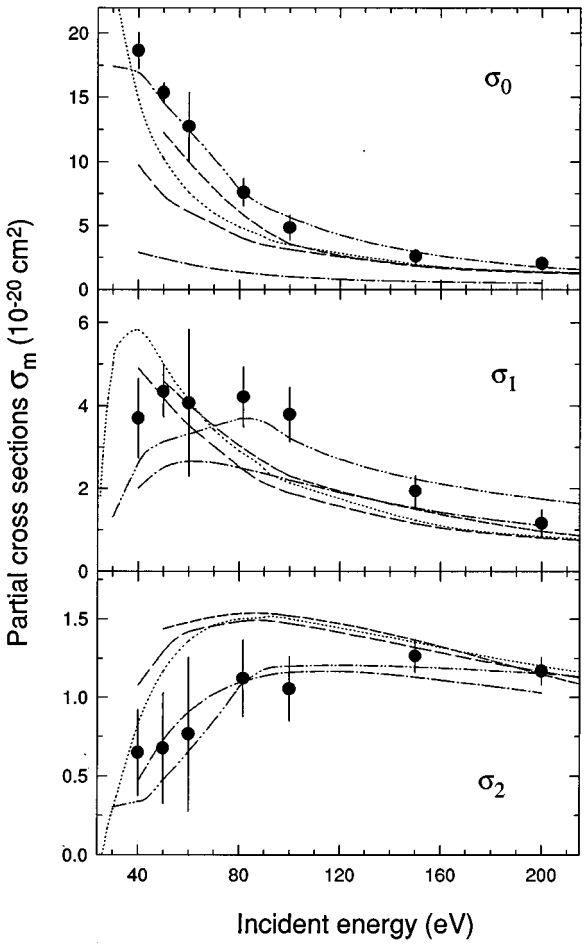

FIG. 5. Partial cross sections σ_m ($m=0,\pm1,\pm2$) vs incident energy. Experiment: present results (●). Theory: ten-state eikonal calculations (long-dashed line, Ref. [27]), 22-state second-order diagonalization method (short-dashed line, Ref. [21]), multichannel eikonal theory (dotted line, Ref. [23]), distorted-wave Born approximation with excited-state distorting potentials (dash-dotted line, Ref. [24]), and convergent close-coupling theory (dash-dot-dot line, Ref. [27]).

general, the predicted degree of linear polarization $P_1^{(\gamma_1)}$ is 10–20 % smaller than experimentally observed. This indicates from Eq. (7) that the difference $(\sigma_0+\sigma_1)-2\sigma_2$ is underestimated in the calculations. The new CCC calculated values of Fursa and Bray [27] are again in excellent agreement with the measurements, except at energies below 50 eV, where minor discrepancies seem to persist.

More insight into the collision process is provided by the partial cross section σ_m for excitation of the He($3\,^1D$) magnetic substates ($m=0,\pm1,\pm2$) that are displayed in Fig. 5. At low-incident energies, σ_0 is by far the largest while σ_2 is smallest. Towards larger energies, σ_0 decreases rather rapidly while the other two partial cross sections, σ_1 and σ_2 appear to attain broad maxima around 70 and 150 eV, respectively. The theoretical calculations based on the various models [21–24,27] are in qualitative agreement with this behavior as they predict a monotonic decreasing partial cross section σ_0 in the range above 40 eV. On a quantitative basis, σ_0 appears to be larger compared to most calculations [21–24] with the exception of the convergent close-coupling cal-

culation [27], which agrees excellently with our data. Large deviations to most calculations are also noted for σ_1. While the experimental data suggest an almost constant σ_1 from about 40 to 100 eV, the 22-state second-order diagonalization method (SOD) [21], ten-state eikonal calculation [22], and the multichannel eikonal theory (DMET) [23] all predict a cross section that peaks below or around 40 eV. Cross-section maxima at larger energies around 60 and 80 eV, respectively, are predicted by the DWBA-EP and the CCC method [24,27]. Again, the agreement between experiment and theory is very good for the CCC calculations, while large deviations are noted for the other calculations. The magnitude of the partial cross section σ_2 around 100 eV and the position of the cross-section maximum is not well reproduced by the SOD, eikonal, and DMET theories [21–23]. This indicates that these theories do not properly account for collisions with large momentum transfer. Good agreement is obtained here with the DWBA-EP and the CCC theories [24,27].

The above data, in conjunction with Eqs. (7) and (9), permit the following picture of the collision process. Only the CCC model includes full coupling to continuum and other bound states and that coupling is important, as shown by Figs. 4 and 5. It causes the sum $(\sigma_0+\sigma_1)$ to be larger, and $2\sigma_2$ to be lower, than other theories at most energies. The combination of the σ_m in Eq. (7) accounts for the general energy dependence of the linear polarization shown in Fig. 4 and also indicates that the linear polarization will become negative above about 300 eV because $(\sigma_0+\sigma_1)$ is decreasing more quickly than $2\sigma_2$.

The data indicate that σ_0, that is, collisions with $\Delta m=0$, dominate at energies less than about 80 eV. This result is in agreement with the earlier data on the Stokes parameters from our laboratory [30], which indicated an electron-charge cloud of a predominantly $|d_0\rangle$ state lying in the scattering plane. At higher energies σ_0 becomes comparable with σ_1, and by about 300 eV they are comparable with σ_2. The $\langle t_{40}\rangle$ multipole, see Table I, reaches a near-zero minimum near 100 eV and, through Eq. (9c), for which $(3\sigma_0+\sigma_2)=4\sigma_1$, one may expect a change in the nature of the collision process because of the relatively higher value of σ_2. Further measurements of the Stokes parameters would clarify this behavior.

In summary, the present experimental results for the partial cross sections σ_m $(m=0,\pm1,\pm2)$ obtained with a polarized first-photon–second-photon coincidence technique are found to be in excellent agreement with the most recent convergent close-coupling (CCC) calculations of Fursa and Bray [27], but disagree with the other available calculations based on different (SOD, eikonal, DMET, and DWBA-EP) methods [21–24]. This technique and the results obtained with it thus stringently test existing theoretical calculations and are, therefore, helpful in obtaining a deeper understanding of these fundamental collision processes.

ACKNOWLEDGMENTS

This research was supported by The Australian Research Council (ARC) and The University of Western Australia (UWA). A.G.M. was financially supported by the ARC. R.H. would like to thank The University of Western Australia for its hospitality and the ARC. The authors would like to thank Don Madison (Rolla), Igor Bray (Adelaide), and Andris Stelbovics (Murdoch) for valuable discussions.

[1] N. Andersen, W. Gallagher, and I. V. Hertel, Phys Rep. **165**, 1 (1988).
[2] A. G. Mikosza, J. F. Williams, R. Hippler, J. B. Wang, and P. A. Smith, *XIX International Conference on the Physics Electronic and Atomic Collisions Abstracts*, edited by L. Dube, J. B. Mitchell, J. W. McConkey, and C. E. Brion (AIP, Woodbury, 1995).
[3] J. F. Williams, M. Kumar, and A. T. Stelbovics, Phys. Rev. Lett. **70**, 1240 (1993).
[4] A. Mikosza, R. Hippler, J. B. Wang, and J. F. Williams, Phys. Rev. Lett. **71**, 235 (1993).
[5] J. B. Wang, J. F. Williams, A. T. Stelbovics, J. E. Furst, and D. H. Madison, Phys. Rev. A **52**, 2885 (1995).
[6] U. Fano and J. H. Macek, Rev. Mod. Phys. **45**, 553 (1973).
[7] K. Blum and H. Kleinpoppen, Phys. Rep. **52**, 203 (1979).
[8] K. Blum, *Density Matrix Theory and its Application* (Plenum, New York, 1981).
[9] E. I. Heck and J. Gauntlett, J. Phys. B **19**, 3633 (1986).
[10] A. R. Edmonds, *Angular Momentum in Quantum Mechanics* (Princeton University Press, Princeton, 1960).
[11] M. Hollywood, A. Crowe, and J. F. Williams, J. Phys. B **12**, 819 (1979); I. Humphrey, J. F. Williams, and E. L. Heck, *ibid.* **20**, 367 (1987).
[12] A. G. Mikosza, R. Hippler, J. B. Wang, J. F. Williams, and A. B. Wedding, J. Phys. B **27**, 1429 (1994).
[13] A. B. Wedding, A. G. Mikosza, and J. F. Williams, J. Opt. Soc. Am. A **8**, 1729 (1991).
[14] D. T. McLaughlin and A. Crowe, J. Phys. B **25**, 5171 (1992).
[15] A. H. Gabriel and D. W. O. Heddle, Proc. R. Soc. London A **258**, 124 (1960).
[16] R. M. St. John, F. L. Miller, and C. C. Lin, Phys. Rev. **134**, A888 (1964).
[17] H. R. M. Moussa, F. J. de Heer, and J. Schutten, Physica **40**, 517 (1969).
[18] J. G. Showalter and R. B. Kay, Phys. Rev. A **11**, 1899 (1975).
[19] L. Vriens and J. D. Carriére, Physica **49**, 517 (1970).
[20] K. L. Bell, D. J. Kennedy, and A. E. Kingston, J. Phys. B **2**, 26 (1969).
[21] D. Baye and P.-H. Heenen, J. Phys. B **7**, 938 (1974).
[22] M. R. Flannery and K. J. Cann, J. Phys. B **8**, 716 (1975).
[23] E. J. Mansky and M. R. Flannery, J. Phys. B **23**, 3987; **23**, 4573 (1990).
[24] Own calculations using a computer code kindly provided by K. Bartschat and D. H. Madison, J. Phys. B **21**, 153 (1988).
[25] F. J. de Heer, R. Hoekstra, A. E. Kingston, and H. P. Summers, *Nuclear Fusion* (International Atomic Energy Agency, Vienna, 1992), Vol. 3, p. 19.

[26] T. Kato and R. K. Janev, *Nuclear Fusion* (International Atomic Energy Agency, Vienna, 1992), Vol. 3, p. 33.
[27] D. V. Fursa and I. Bray, Phys. Rev. A **52**, 1279 (1995), and private communication.
[28] I. Bray and A. Stelbovics, Phys. Rev. A **46**, 6995 (1992).
[29] G. Csanak and D. C. Cartwright, J. Phys. B **22**, 2769 (1989).
[30] A. Mikosza, R. Hippler, J. B. Wang, and J. F. Williams, Z. Phys. D **30**, 129 (1994).